OPTIMIZATION OF THE INFLUENCE OF TEMPERATURE ON THE ELECTRICAL DISTRIBUTION OF STRUCTURES WITH RADIAL p-n JUNCTION STRUCTURES

Jo'shqin Sh. Abdullayev[a]*, Ibrokhim B. Sapaev[a,b]

[a]National Research University TIIAME, Department of Physics and Chemistry, Tashkent, Uzbekistan
[b]Western Caspian University, Scientific researcher, Baku, Azerbaijan
*Corresponding Author e-mail: j.sh.abdullayev6@gmail.com

In recent years, advances in optoelectronics and electronics have prioritized optimizing semiconductor device performance and reducing power consumption by modeling new semiconductor device geometries. One such innovative structure is the radial p-n junction structure. In this work, we present a concept that submicron three-dimensional simulations were conducted on radial p-n junction structures based on GaAs material to investigate the influence of temperature ranging from 250K to 500K with a step of 50K on the electrophysical distribution, such as space charge, electro-potential, and electric field, in radial p-n junction structures, as well as various forward voltages. In particular, we focus on the shell radius within the structure: 0.5 μm and 1 μm for the shell. The modeling results were compared with the results obtained from solving the theoretical Poisson equation in the cylindrical coordinate system.

Keywords: *Core-shell; Radial p-n junction; Cylindrical coordinates; Space charge density; Gallium Arsenide (GaAs)*
PACS: 73.40.Lq, 73.61.Cw, 73.61.Ey, 72.20.Jv

INTRODUCTION

Until now, modern scientific publications on semiconductor electronic devices have mainly focused on planar structures of p-n and p-i-n junction structures. On the other side, in recent years, theoretical [1-3] and practical [4,5] studies and modeling semiconductor devices, have made it possible to explore new geometric configurations, revealing intriguing and unexplored electrical properties. One such configuration is the radial structures of p-n and p-i-n junction structures and so on.

Although planar p-n and p-i-n junction structures offer numerous advantages, such as ease of fabrication, they also have limitations, such as limited active surface area [6]. This limitation can impact performance in applications where intense charge carrier interactions are critical such as detectors [7]. Additionally, in optoelectronic devices, planar p-n and p-i-n junction structures may exhibit limited light-matter interactions compared to their 3D counterparts [8].

Hence, studying the electrical and optical characteristics of novel geometric structures becomes essential. Radial designs of p-n and p-i-n junctions offer several advantages compared to their flat counterparts. First, radial p-n and p-i-n junction structures offer increased surface area, which improves the interaction between charge carriers and potentially improves device performance [9]. Moreover, in some photonic applications, radial structures exhibit superior light absorption characteristics compared to planar structures. Additionally, radial configurations can reduce series resistance, thereby increasing the overall efficiency of the device [10]. Indeed, depending on the intended application of the semiconductor electronic devices, the implementation of various modifications can lead to new effects and further advances. Hence, the study of the electrophysical and optoelectrical features of radial p-n and p-i-n junction structures is becoming a critical area of research. Experimental methods for growing radial p-n and p-i-n junction structures using GaAs material have been studied for several research purposes [11-14].

Various methods for fabricating radial pn junction structures have emerged, including vapor-liquid-solid (VLS) [15], chemical vapor deposition (CVD) [16], and plasma-enhanced chemical vapor deposition (PECVD), [17] and metal chemical etching (MACE) [18]. Using these techniques, researchers have successfully created structures such as nanowire arrays [19], nanocones [20], and micropillars [21] designed for enhanced light absorption in radial p-n and p-i-n junction configurations.

This arrangement provides many advantages. For example, the design of a radial p-n junction aligns the direction of light absorption perpendicular to the direction of minority carrier transport. This configuration allows the cell to maintain sufficient thickness to effectively absorb light while simultaneously providing a short path for carrier collection. This design is suitable for highly integrated optoelectronic devices such as solar cells [22], biosensors, memories [23], light emitting diodes (LEDs) [24], radial photodiodes, high electron mobility transistors [25] and field effect transistors [26].

Despite significant advances in the theory and application of radial p-n junctions and p-i-n junctions, unresolved problems remain, especially regarding the electrophysical distributions, such as space charge density, electric potential, and electric field, in radial p-n junction structures as well as various forward voltages at different radii and over a wide temperature range. In addition, the injection of minority charge carriers has practically not been studied in scientific works. The electrophysical distributions in planar p-n and p-i-n junction structures intended for sensor devices have been extensively studied [27]. However, the electrophysical distributions in radial p-n and p-i-n junction structures have not

been fully explored. Hence, it is imperative to investigate the dependence of electrophysical distributions in radial p-n and p-i-n junction structures on various external parameters.

Thus, our research efforts in this work are focused on the in-depth study and modeling of the electrical properties of radial p-n junction structures using GaAs material, known for its bandgap suitability for optoelectronic devices. Given the wide bandgap of GaAs (Eg = 1.42eV), it is widely used in semiconductor optoelectronics. The simulation results are compared with the solutions obtained by solving the Poisson equation in a cylindrical coordinate system at different temperatures [28]. Section METHODS AND MATERIAL provides an overview of the sample geometry, and material characteristics, as well as methodological studies of the distribution of space charge density, electric potential, and electric field. Section RESULTS AND DISCUSSION details the results of our new model and discusses its implications.

METHODS AND MATERIAL

In this study, submicron three-dimensional simulations were conducted on radial p-n junction structures based on GaAs material to investigate the influence of temperature ranging from 250K to 500K with a step of 50K on the electrophysical distribution, such as space charge, electro-potential, and electric field, in radial p-n junction structures, as well as from 0 to 1 Volt forward voltages. In particular, we focus on the shell radius within the structure: 0.5 μm and 1 μm for the shell.

METHODS AND THEORETICAL BACKGROUND

At the same time, it is required to solve the Poisson equation to determine the appearance of electrophysical distributions in the Panar and Radial p-n and p-i-n transition structures and to study the influence of external factors on the electrophysical distributions. Taking into account that electrophysical distributions in radial p-n and p-i-n junction structures and the mechanism of current flow in them are hardly studied, we solve Poisson's equation in the cylindrical coordinate system. The three-dimensional Poisson's equation in cylindrical coordinates is given by Eq. (1):

$$\frac{\partial^2 \varphi(r)}{\partial r^2} + \frac{1}{r}\frac{\partial \varphi(r)}{\partial r} + \frac{1}{r^2}\frac{\partial^2 \varphi(r)}{\partial \theta^2} + \frac{\partial^2 \varphi(r)}{\partial z^2} = -\frac{\rho(r,\theta,z)}{\varepsilon\varepsilon_0} \tag{1}$$

Here, r represents the radial dimension, z denotes an axial dimension, θ signifies an azimuthal angle, $\rho(r)$ represents charge density, and $\varphi(r)$ stands for electrostatic potential. If Poisson's equation is expressed solely for one radial dimension, it appears as follows Eq. (2a) and (2b):

$$\frac{\partial^2 \varphi(r)}{\partial r^2} + \frac{1}{r}\frac{\partial \varphi(r)}{\partial r} = -\frac{\rho(r)}{\varepsilon\varepsilon_0} \tag{2a}$$

$$\frac{dE(r)}{dr} + \frac{dE(r)}{r} = \frac{\rho(r)}{\varepsilon\varepsilon_0} \tag{2b}$$

Where $E(r)$ represents the electric field, ε denotes the permittivity of the semiconductor material, for GaAs ε is 12.9, $\varepsilon_0 = 8.85 \cdot 10^{-12}$ F·m^{-1} vacuum permittivity. By solving the second-order differential equation, we can determine the following distributions in the radial dimension from Eq. (3a) and (3b): $\rho(r)$ represents the charge density, $\varphi(r)$ denotes the electrostatic potential, and $E(r)$ signifies the electric field. Through this process, distributions in radial p-n and p-i-n junction structures can be determined.

$$\varphi(r) = -\frac{\rho(r)\cdot r^2}{4\varepsilon\varepsilon_0} + C_1 \cdot \ln(r) + C_2 \tag{3a}$$

$$E(r) = -\frac{d\varphi(r)}{dr} = \frac{\rho(r)\cdot r}{2\varepsilon\varepsilon_0} - \frac{C_1}{r}. \tag{3b}$$

To achieve this, it is necessary to establish the initial and boundary conditions for solving the second-order differential equation, identify C_1 and C_2, and find the solutions individually of electrostatic potential and electric field. We introduce the conditions as follows: $E(R/2+r_n)=0$, $E(R/2-r_p)=0$, $\varphi(R/2-r_p)=0$ $\varphi(R/2+r_n)=\varphi_k$. Here φ_k is built potential, for $\varphi_k =1.28$ Volt GaAs, r_n and r_p are border radial dimensions of depletion region respectively core (p-type) and shell (n-type) side. See Figure 1 to understand the radial distance here.

$$E(-R \leq r < -r_n) = 0 \text{ and } E(0 \leq r < r_p) = 0 \tag{5a}$$

$$E(r_p < r < r_n) = \frac{qN_A}{2\varepsilon\varepsilon_0}(r+r_p) \tag{5b}$$

$$E(-r_p < r < -r_n) = -\frac{qN_D}{2\varepsilon\varepsilon_0}(r - r_n)$$ (5c)

$$E(-r_p < r \le 0) = 0 \text{ and } E(r_n < r \le R) = 0$$ (5d)

Expressions (5a), (5b), (5c), and (5d) are obtained by solving expression (3b) using integrals with the initial conditions stated above. The solutions to these derived equations are presented graphically in Figure 4. The graphs in the next section were obtained from the solutions of these equations. Here, Majority carrier concentration $p_p = n_n = N_A = N_D = 2 \cdot 10^{16}$ cm^{-3}, minority carrier concentration $p_n = \frac{n_i^2}{N_D}$, $n_p = \frac{n_i^2}{N_A}$. Here n_i is instrinsic concentration, $n_i = 1.7 \cdot 10^6$ cm^{-3} for GaAS. Electrons and holes mobility $\mu_n = 8500 \left[\frac{cm^2}{V \cdot s} \right]$ and $\mu_p = 400 \left[\frac{cm^2}{V \cdot s} \right]$ for GaAs align closely with their respective literature values and the functional parameters of GaAs material are sourced from the following literature [29].
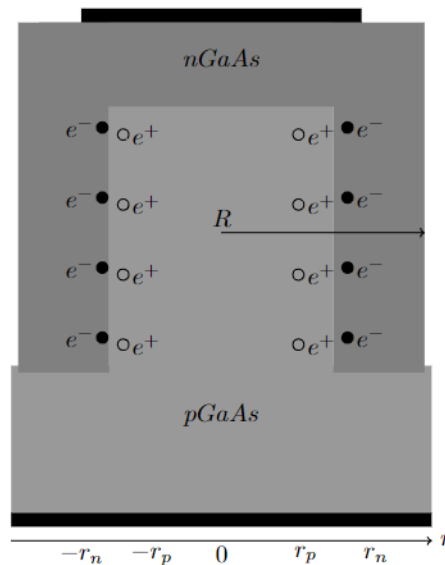

Figure 1. 2D cross-section of the radial p-n junction. The light grey area signifies the p-type GaAs, while the dark grey area represents the n-type GaAs. The black field indicates the Ohmic contact prepared with Al. Here e^- and e^+ denote electrons and holes respectively, while r denotes the radial dimension. R is the radius of the shell.

We aim to explore the electrophysical characteristics of an individual radial p-n junction structure at a submicron scale, considering both the periodic recurrence of radial structures within submicron dimensions and the cyclical nature of electrophysical processes occurring within them. In this paper, we assume that donor and acceptor ions are completely ionized within the chosen temperature range. Additionally, we have selected the symmetric p-n junction with complete ionization, where p = n = N$_A$= N$_D$=2e16 cm^{-3}. In particular, we focus on the core and shell radii within the structure: R=0.5 μm and R=1 μm for the shell. In both cases, the core radius, denoted by R/2 is chosen to be equal to half the shell radius. This choice enables us to consider the symmetric electrical distribution. Semiconductor electronic devices heavily depend on the operational efficiency of the p-n junction. Therefore, this study is dedicated to examining the electrical distribution occurring within the radial p-n junction. We did not include the electrical distribution within the substrate in this analysis. The results obtained from the models and samples employed in this section are thoroughly presented and scrutinized in Section RESULTS AND DISCUSSION.

RESULTS AND DISCUSSION

This section presents graphs illustrating the variations of current I with voltage U and their analysis as the temperature changes from 250K to 500K in 50K increments. Additionally, it includes distributions of electrophysical properties such as space charge density, electrostatic potential, and electric field.

Distributions of Electrophysical Parameters

The maximum value of charge density is dependent on doping concentration and is not influenced by geometric parameters by Equation (2). Hence, So, regardless of whether the radius is 0.5 μm or 1 μm, the maximum value of charge density remains the same. Indeed, the change in radius alters the charge distribution in radial p-n junction structures, as illustrated in Figure 2. The change in charge distribution within the core-shell terminal is observed from -0.8 μm to -0.4 μm and from 0.4 μm to 0.8 μm d~0.4 μm within the depletion region thickness, d is representing the depth of the depletion region. With the increase in temperature, the charge density of carriers also increases.
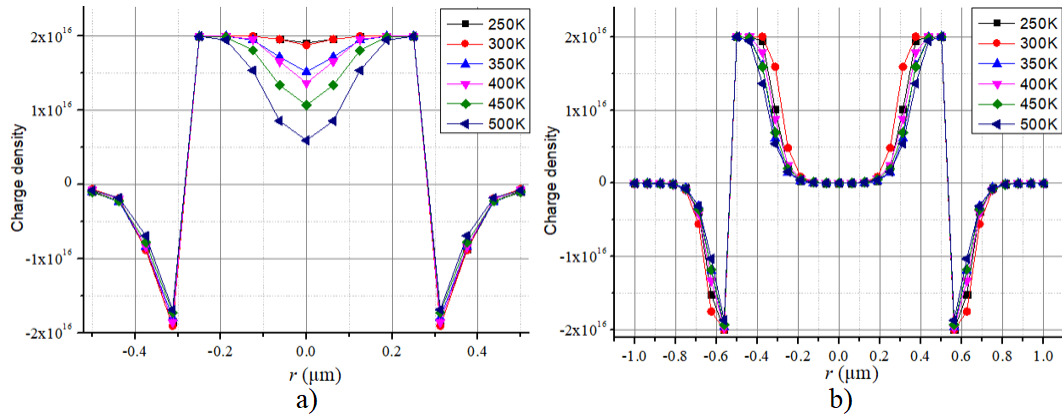
Figure 2. Distribution of space charge density $\rho(r)$ [cm^{-3}] across radial p-n junction structure by radial dimension
a) corresponding to R =0.5 μm and b) corresponding to R =1 μm based on GaAs.

In Figure 2, it's evident that the charge distribution within the thickness of the shell remains uniform for both R=0.5 μm and 1 μm, whereas it varies within the thickness of the core. This observation can be attributed to the difference in charge distribution within the core, which ultimately constrains the charge density [30-33]. The distribution of electrostatic potential under the influence of forward voltage shows that potential changes are predominantly observed in the depleted regions of both the core and shell. Other areas show minimal changes.

From the expression for $E(r) = -d\varphi(r)/dr$ it's evident that the electrostatic field reaches its maximum value at locations where changes in charge density and electrostatic potential occur, as depicted in Figures 2 and 3. Additionally, the electrostatic field increases with rising temperature and the radius of the shell.
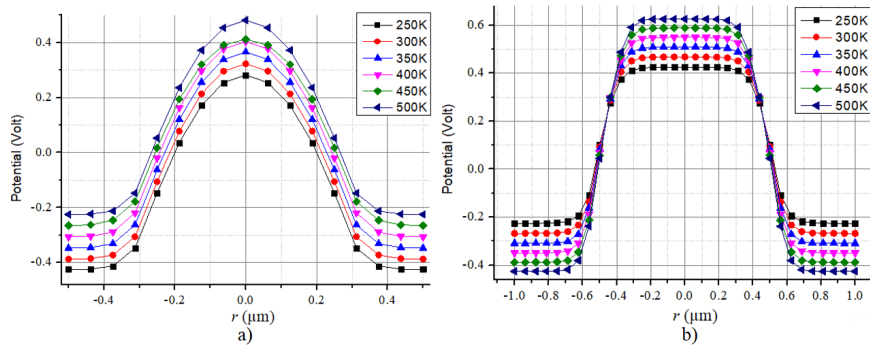

Figure 3. Distribution of Electrostatic potential $\varphi(r)$ across radial p-n junction structures by radial dimension
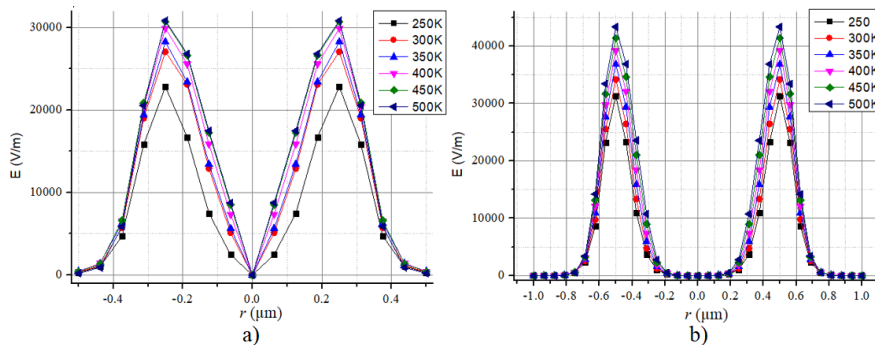a) corresponding to R =0.5 μm and b) corresponding to R =1 μm based on GaAs.

Figure 4. Distribution of Electric field $E(r)$ across radial p-n junction structures by radial dimension in 1D system
a) corresponding to R =0.5 μm and b) corresponding to R =1 μm based on GaAs.

It represents the dependence of the electric field distribution on the 1D radial dimension, showing that the electric field has a high value at the p-n junction. In case a) corresponding to R= 0.5 μm, the electric field value is 30 kV/m, while in case b) at R=1 μm, the electric field reaches a maximum value of 45 kV/m. To explain this situation, we approach it as follows: the change in electrostatic potential and the value of the space charge density are considered by taking a large value.

Analyze I-U-T Curves

The current transport mechanism in p-n junction structures can often be discerned by analyzing the representation of the I-U curve on a semi-logarithmic graph. Therefore, we illustrated a semi-logarithmic I-U curve in Figure 3. Upon

observing the volt-ampere characteristics, it becomes evident that the current transport mechanism remains consistent despite variations in radius. However, the current values vary, a phenomenon attributed to changes in geometric size. In semiconductor electronic devices, the analysis of the I-U curve is critical for assessing the quality of the selected sample for a model. This curve provides valuable insights into the device's performance, aiding in the identification of any irregularities or inefficiencies that may affect its functionality. The semi-logarithmic scale of the I-U curve can fully elucidate the current flow mechanism, hence its utilization in our representation. However, a noteworthy observation reveals that the current transport mechanism does change with temperature variations. Figure 5 demonstrates this phenomenon: At low voltages up to 0.4 V, the recombination-generation mechanism predominates. In the voltage range from 0.4 to 0.8 V, the drift-diffusion mechanism prevails. Beyond these ranges, the phenomenon of high injection is observed, extending up to 1 volt.
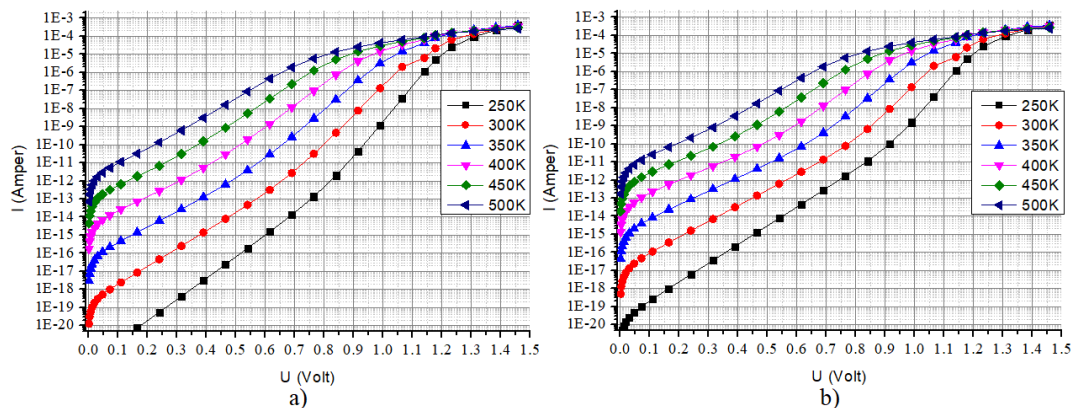

Figure 5. depicts the semi-logarithmic current-voltage characteristics for a GaAs-based p-n junction, with a) R=0.5 μm and b) R =1 μm respectively.

At homogeneous values of temperature and forward voltage, at different values of radius R=0.5 μm and R=1 μm, the current transport mechanism remained unchanged, and the value of the current increased. This situation can be explained by the increase of the current passing active surface with the change of geometric size.

CONCLUSIONS

In summary, the maximum value of the charge density depends on the doping concentration and is independent of geometric parameters. This finding suggests that both nano- and micro-scale pn junctions exhibit the same maximum charge density at equivalent concentrations. Under uniform temperature and forward voltage conditions, different radii (R=0.5 μm and R=1 μm) do not alter the current transfer mechanism, but they do increase the current value. This can be attributed to the increase in the current-carrying active surface area with changes in geometric size. Analysis of the I-U curve in the model reveals that the current transport mechanism remains consistent across different radii in radial p-n junction structures. However, an interesting observation indicates that the current transport mechanism does change with temperature variations. In Figure 5, I-U curve 5 illustrates that at low voltages (up to 0.4 V), the recombination-generation mechanism predominates, while in the range of 0.4 to 0.8 V, the drift-diffusion mechanism prevails. In other cases, the phenomenon of high injection is observed up to 1 volt. In future studies, we will explore the C-U characteristic using this model.

ORCID

Jo'shqin Sh. Abdullayev, https://orcid.org/0000-0001-6110-6616; **Ibrokhim B. Sapaev,** https://orcid.org/0000-0003-2365-1554

REFERENCES

[1] Sh. Qian, S. Misra, J. Lu, Z. Yu, L. Yu, J. Xu. J. Wang, *et al*., Appl. Phys. Lett. **107**, 043902 (2015). https://doi.org/10.1063/1.4926991
[2] E. Gnani, A. Gnudi, S. Reggiani, and G. Baccarani, IEEE Trans. Electron Devices, **58**(9), 2903 (2011). https://doi.org/10.1109/TED.2011.2159608
[3] Z. Arefinia, A. Asgari, Solar Energy Materials and Solar Cells, **137**, 146 (2015). https://doi.org/10.1016/j.solmat.2015.01.032
[4] O.V. Pylypova, A.A. Evtukh, P.V. Parfenyuk, I.I. Ivanov, I.M. Korobchuk, O.O. Havryliuk, and O.Yu. Semchuk, Opto-Electronics Review, **27**(2), 143 (2019). https://doi.org/10.1016/j.opelre.2019.05.003
[5] R. Ragi, R.V.T. da Nobrega, U.R. Duarte, and M.A. Romero, IEEE Trans. Nanotechnol. **15**(4), 627 (2016). https://doi.org/10.1109/TNANO.2016.2567323
[6] R.D. Trevisoli, R.T. Doria, M. de Souza, S. Das, I. Ferain, and M.A. Pavanello, IEEE Trans. Electron Devices, **59**(12), 3510 (2012). https://doi.org/10.1109/TED.2012.2219055
[7] N.D. Akhavan, I. Ferain, P. Razavi, R. Yu, and J.-P. Colinge, Appl. Phys. Lett. **98**(10), 103510 (2011). https://doi.org/10.1063/1.3559625
[8] A.V. Babichev, H. Zhang, P. Lavenus, F.H. Julien, A.Y. Egorov, Y.T. Lin, and M. Tchernycheva, Applied Physics Letters, **103**(20), 201103 (2013). https://doi.org/10.1063/1.4829756

[9]   D.H.K. Murthy, T. Xu, W.H. Chen, A.J. Houtepen, T.J. Savenije, L.D.A. Siebbeles, *et al*., Nanotechnology, **22**(31), 315710 (2011). https://doi.org/10.1088/0957-4484/22/31/315710

[10] B. Pal, K.J. Sarkar, and P. Banerji, Solar Energy Materials and Solar Cells, **204**, 110217 (2020). https://doi.org/10.1016/j.solmat.2019.110217

[11] I. Aberg, G. Vescovi, D. Asoli, U. Naseem, J.P. Gilboy, C. Sundvall, and L. Samuelson, IEEE Journal of Photovoltaics, **6**(1), 185 (2016). https://doi.org/10.1109/JPHOTOV.2015.2484967

[12] P. Dubey, B. Kaushik, and E. Simoen, IET Circuits, Devices & Systems, (2019). https://doi.org/10.1049/iet-cds.2018.5169

[13] M.-D. Ko, T. Rim, K. Kim, M. Meyyappan, and C.-K. Baek, Scientific Reports, **5**(1), 11646 (2015). https://doi.org/10.1038/srep11646

[14] A.M. de Souza, D.R. Celino, R. Ragi, and M.A. Romero, Microelectronics J. **119**, 105324 (2021). https://doi.org/10.1016/j.mejo.2021.105324

[15] M.C. Putnam, S.W. Boettcher, M.D. Kelzenberg, D.B. Turner-Evans, J.M. Spurgeon, E.L. Warren, *et al*., Energy & Environmental Science, **3**(8), 1037 (2010). https://doi.org/10.1039/C0EE00014K

[16] S. Osono, Y. Uchiyama, M. Kitazoe, K. Saito, M. Hayama, A. Masuda, A. Izumi, *et al*., Thin Solid Films, **430**, 165 (2003). https://doi.org/10.1016/S0040-6090(03)00100-7

[17] R. Elbersen, R.M. Tiggelaar, A. Milbrat, G. Mul, H. Gardeniers, and J. Huskens, Advanced Energy Materials, **5**(6), 1401745 (2014). https://doi.org/10.1002/aenm.201401745

[18] A.A. Leonardi, M.J.L. Faro, and A. Irrera, A Review. Nanomaterials, **11**(2), 383 (2021). https://doi.org/10.3390/nano11020383

[19] A. Yesayan, F. Jazaeri, and J.-M. Sallese, IEEE Trans. Electron Devices, **63**(3), 1368 (2016). https://doi.org/10.1109/TED.2016.2521359

[20] Y. Li, M. Li, P. Fu, R. Li, D. Song, C. Shen, and Y. Zhao, Scientific Reports, **5**(1), 11532 (2015). https://doi.org/10.1038/srep11532

[21] J.C. Shin, D. Chanda, W. Chern, K.J. Yu, J.A. Rogers, and X. Li, IEEE Journal of Photovoltaics, **2**(2), 129 (2012). https://doi.org/10.1109/JPHOTOV.2011.2180894

[22] D. Choi, and K. Seo, Advanced Energy Materials, **11**(5), 2003707 (2021). https://doi.org/10.1002/aenm.202003707

[23] M. Shahram, T. Iman, and N.R. Mahdiyar, Optical and Quantum Electronics, **54**(2), 115 (2022). https://doi.org/10.1007/s11082-021-03499-2

[24] Bryan Melanson, M. Hartensveld, C. Liu, and J. Zhang, AIP Advances, **11**(9), 095005 (2021). https://doi.org/10.1063/5.0061381

[25] Y. Xiao, B. Zhang, H. Lou, L. Zhang, and X. Lin, IEEE Trans. Electron Devices, **63**(5), 2176 (2016). https://doi.org/10.1109/TED.2016.2535247

[26] B. Liu, J. Wang, Z. Li, Z. Sun, C. Li, J.-M. Seo, J. Li, *et al*., Nano Energy, **126**, 109611 (2024). https://doi.org/10.1016/j.nanoen.2024.109611

[27] R.K. Patnaik, and D.P. Pattnaik, in: *2016 International Conference on Signal Processing, Communication, Power and Embedded Systems (SCOPES)*, (Paralakhemundi, India, 2016). https://doi.org/10.1109/SCOPES.2016.7955628

[28] A.C.E. Chia, and R.R. LaPierre, J. Appl. Phys. **112**, 063705 (2012). https://doi.org/10.1063/1.4752873

[29] S.M. Sze, and K.K. Ng, *Physics of Semiconductor Devices*, Third Edition, (John Wiley & Sons, Inc., 2007).

[30] G.E. Cirlin, V.G. Dubrovskii, I.P. Soshnikov, N.V. Sibirev, Y.B. Samsonenko, A.D. Bouravleuv, J.C. Harmand, *et al*., Phys. Status Solidi (RRL), **3**, 112 (2009). https://doi.org/10.1002/pssr.200903057

[31] T.J. Kempa, R.W. Day, S.-K. Kim, H.-G. Park, and C.M. Lieber, Energy Environ. Sci. **6**(3), 719 (2013). https://doi.org/10.1039/c3ee24182c

[32] M.I. Khan, I.K.M.R. Rahman, and Q.D.M. Khosru, IEEE Trans. Electron Devices, **67**(9), 3568 (2020). https://doi.org/10.1109/TED.2020.3011645

[33] D.R. Bachman, S.E. Park, S. Thaveepunsan, J.S. Fitzsimmons, K.-N. An, and S.W. O'Driscoll, Journal of Orthopaedic Trauma, 1 (2018). https://doi.org/10.1097/BOT.0000000000001278

ОПТИМІЗАЦІЯ ВПЛИВУ ТЕМПЕРАТУРИ НА ЕЛЕКТРИЧНИЙ РОЗПОДІЛ КОНСТРУКЦІЙ ІЗ РАДІАЛЬНИМИ СТРУКТУРАМИ P-N ПЕРЕХОДУ

Джошкін Ш. Абдуллаєв[a], Іброхім Б. Сапаєв[a,b]

[a]Національний дослідницький університет ТІАМЕ, фізико-хімічний факультет, Ташкент, Узбекистан
[b]Західно-Каспійський університет, науковий співробітник, Баку, Азербайджан

Останніми роками досягнення в оптоелектроніці та електроніці віддають перевагу оптимізації продуктивності напівпровідникових пристроїв і зниженню енергоспоживання шляхом моделювання нових геометрій напівпровідникових пристроїв. Однією з таких інноваційних структур є структура радіального p-n переходу. У цій роботі ми представляємо концепцію, згідно з якою субмікронне тривимірне моделювання було проведено на структурах радіального p-n-переходу на основі матеріалу GaAs для дослідження впливу температури в діапазоні від 250 K до 500 K з кроком 50 K на електрофізичний розподіл, такий як просторовий заряд , електропотенціал і електричне поле в структурах радіального p-n переходу, а також різні прямі напруги. Зокрема, ми зосереджуємося на радіусі оболонки всередині конструкції: 0,5 μm і 1 μm для оболонки. Результати моделювання порівнювали з результатами, отриманими при розв'язуванні теоретичного рівняння Пуассона в циліндричній системі координат.

Ключові слова: *ядро-оболонка, радіальний p-n-перехід; циліндричні координати; просторова густина заряду; арсенід галію (GaAs)*